Journal of Ship Research, Vol. 66, No. 1, March 2022, pp. 1–14
http://dx.doi.org/10.5957/JOSR.04200028

Journal of
Ship Research

Enhanced Unified Theory with Forward-Speed Effect Taken into Account in the Inner Free-Surface Condition

Masashi Kashiwagi

Department of Naval Architecture and Ocean Engineering, Osaka University, Osaka, Japan

The enhanced unified theory (EUT) has been used as a core theory in the integrated system developed at the Research Initiative on Oceangoing Ships (RIOS) of Osaka University for predicting the propulsion and seakeeping performance of a ship in actual seas. In this study, the EUT is modified by adopting partially the solution method in the rational strip theory of Ogilvie and Tuck as a particular solution in the inner problem, thereby a forward-speed effect in the convection term of the free-surface condition is incorporated in the inner solution. This forward-speed effect is analytically shown to contribute only to the cross-coupling radiation forces. Some other forward-speed and 3D effects important in a low-frequency range are also included in the homogeneous component of the inner solution through matching with the outer solution in a similar manner to the unified theory of Newman. Numerical computations are implemented for a slender modified Wigley model and the RIOS bulk carrier model. Good agreement is confirmed in a comparison with experimental data for the cross-coupling added mass and damping coefficients between heave and pitch and also for the resulting ship motions, particularly in heave near the resonant frequency. The added resistance around the motion-resonant wavelength is found to be improved but sensitive to a slight change in heave and pitch motions. Thus, it is stressed that accurate prediction of the ship motions and resultant Kochin function is critical for more accurate prediction of the added resistance in waves.

Keywords: enhanced unified theory; rational strip theory; cross-coupling radiation force; ship motion; added resistance; forward-speed effect; seakeeping

1. Introduction

Although the design of the ship hull form has been based mainly on the propulsion performance in still water, recently, prediction and onboard data analysis for the propulsion and seakeeping performance of a ship in actual irregular waves have been attracting attention of the researchers (Orihara & Tsujimoto 2018; Minoura et al. 2019). In fact, real ships navigate mostly in rough seas, and thus, the so-called short-term and long-term predictions of ship response in actual seas must be made to guarantee the performance and safety of a ship. This trend to study the seakeeping performance of a ship is partly because the Energy Efficiency Design Index regulation was introduced by International Maritime Organization (IMO) to reduce greenhouse gas emission from the ships in operation. Thus, it becomes important to predict with sufficient accuracy the wave-induced ship motions, the added resistance, and the resultant speed loss of a ship in irregular waves represented by a directional wave spectrum (Kashiwagi 2009; Kim et al. 2017) even in the initial stage of ship design, necessitating computations for various profiles of a candidate ship.

However, in the ship-building community, strip methods have been used for a quick initial prediction of the seakeeping performance with recognition that several shortcomings exist in the theory used. On the other hand, some advanced calculation methods like CFD are available at present (ITTC 2017), but practically, Computational Fluid Dynamics (CFD) methods are time-consuming,

Manuscript received by SNAME headquarters April 26, 2020; accepted for publication September 9, 2020.
Corresponding author: Masashi Kashiwagi, kashi@naoe.eng.osaka-u.ac.jp

despite a fact that they allow studying all nonlinear effects related to large-amplitude motions and fluid viscosity. Moreover, because all physical phenomena are included altogether, it may be hard to understand which components are influential and how and why they are important. El Moctar et al. (2017) studied the added resistance using CFD methods, but they conclude that predicting the wave-induced resistance of ships in waves remains challenging. In the framework of linear potential flow with forward speed, Rankine panel methods (RPM) are popular these days (Kim & Kim 2011; Shao & Faltinsen 2012; Söding et al. 2014 to name a few), but most studies using RPM have been made for regular head waves, and they are still unreliable for low-frequency stern quartering waves and time-consuming if we would compute for all wave directions and frequencies needed for predicting ship responses to irregular waves. Particularly, for the short-term prediction in irregular waves in terms of the spectrum method, the frequency response functions for hydrodynamic quantities concerned must be obtained over a wide range of frequencies and incident wave angles at various ship speeds. Therefore, the calculation method to be used must be fast in computation, reliable in accuracy, and able to deal with practical geometries such as the bulbous bow. These requirements may be satisfied by the enhanced unified theory (EUT) developed by Kashiwagi (1995). With this background, the Research Initiative on Oceangoing Ships (RIOS) at Osaka University has adopted the EUT as a core theory in the integrated prediction and analysis system, in which almost all physical quantities relevant to the seakeeping performance of ships can be computed.

What is important in this prediction system is not only fast computation for various conditions but also we must be able to understand semianalytically whether obtained results are reasonable and which components in the boundary conditions or governing equations are essential for further improvement in the results obtained. This kind of understanding is of critical importance from an academic viewpoint. In that sense, slender ship theories are still valuable and worth revisiting for understanding a relationship, particularly between forward-speed term in the free-surface condition and hydrodynamic-force components in the ship motion equations.

The EUT is based on the slender ship theory and is enhanced from the original unified theory (UT) initiated by Newman (1978) which has brought in 3D effects important for lower frequencies and some forward-speed effects to the 2D strip theory solution. Sclavounos (1984) extended Newman's UT for the radiation problem to the diffraction problem, but the effect of bow wave diffraction was not taken into account. The EUT can analyze the surge-mode radiation problem in the same fashion as that for heave and pitch and also the wave-scattering problem near the ship bow at short waves by retaining the n_x term in the body boundary condition. Consequently, the added resistance can be computed with reasonable accuracy using this EUT. However, notwithstanding relatively good agreement with measured results, it is known as one of the deficiencies that the forward-speed effects in cross-coupling added mass and damping coefficients (particularly between heave and pitch) are not properly accounted for in the EUT (Kashiwagi et al. 2000).

Regarding this deficiency, Ogilvie and Tuck (1969) developed a rational strip theory (RST) in which the free-surface boundary condition in the inner problem close to the ship hull retains not only the zero-speed leading term but also the second leading term that is speed-dependent and is proportional to the parameter $\tau = U\omega/g$ (where U and ω are the forward speed and oscillation circular frequency, respectively, and g is the gravitational acceleration). After comprehensive analysis, it was proven that the solution representing the forward-speed effect linearly proportional to U in the inner free-surface condition contributes eventually only to the cross-coupling added mass and damping coefficients. Numerical computations based on this RST had been implemented by Faltinsen (1974), and very impressive agreement with measured results was found in the cross-coupling terms between heave and pitch. These findings and proof could be achieved for the first time with analytical study, and they are useful information for understanding the physics in computed results to be obtained with large-scale time-consuming computations.

Recalling these results, we recognized that the analysis in the RST of Ogilvie and Tuck (1969) must be adopted as the particular solution in the UT in place of the conventional strip theory solution, and then 3D effects in a low-frequency range must be incorporated through the homogeneous solution as in the original UT. With this idea, the present study proposes a new slender ship theory while keeping the basic theoretical framework of the EUT, and its validity is confirmed by comparison with experiments for the cross-coupling added mass and damping coefficients in heave and pitch; the resulting ship motions in surge, heave, and pitch; and the added resistance in the motion-free condition in head waves. The ship models used for numerical computations and comparison with experiments are a slender modified Wigley model with longitudinal symmetry and the RIOS bulk carrier model with a block coefficient $C_b = .8$.

In this article, Section 2 outlines the formulation, the concept of slender ship theory, resulting outer and inner solutions, and their matching to take account of the forward-speed effect in the inner free-surface boundary condition. In Section 3, the calculation method is described for the cross-coupling radiation forces originating from the forward-speed term in the inner free-surface condition and also briefly for the ship motions and added resistance. Computed results are compared in Section 4 with measured results in the experiment, and discussion is made on the degree of improvement in the ship motions and added resistance by taking account of the forward-speed effect in the inner free-surface condition. Conclusions are given in Section 5.

2. Theory

2.1. Formulation

A ship is assumed to advance at constant forward speed U and oscillate with circular frequency ω in deep water. The right-handed Cartesian coordinate system moving with the ship is chosen, with the x-axis pointing in the direction of forward motion and the z-axis downward. Because there is no outstanding deficiency in the EUT for the diffraction problem, only the radiation problem is considered in this study under the assumption of inviscid fluid with irrotational motion. Then, the velocity potential is introduced and expressed as follows:

$$\Phi(x,y,z,t) = U\Phi_B(x,y,z) + \Re\sum_{j=1}^{6} i\omega X_j \phi_j(x,y,z)e^{i\omega t}. \quad (1)$$

Here, $\Phi_B = -x + \phi_S(x,y,z)$ denotes the steady component of the velocity potential due to ship's steady forward motion at U (thus, ϕ_S is the steady perturbation potential). In this article, Φ_B is taken

as the double-body velocity potential, satisfying the rigid wall condition on $z = 0$. The spatial part $\phi_j(x, y, z)$ in the unsteady component in equation (1) is the radiation potential due to oscillatory motion in the j-th mode with unit velocity; thus, X_j denotes the complex amplitude, where in particular $j = 1$ for surge, $j = 3$ for heave, and $j = 5$ for pitch. The symbol $\Re$ in equation (1) means the real part to be taken.

Assuming small amplitude in the oscillatory motion of a ship, the linearized theory can be used. Then, the body boundary condition to be satisfied by the radiation potential ϕ_j is expressed in the form given as follows:

$$\frac{\partial \phi_j}{\partial n} = n_j + \frac{U}{i\omega} m_j \quad \text{on } S_H, \tag{2}$$

where

$$\left.\begin{aligned} (n_1, n_2, n_3) &= \boldsymbol{n} \\ (n_4, n_5, n_6) &= \boldsymbol{r} \times \boldsymbol{n} \\ (m_1, m_2, m_3) &= -(\boldsymbol{n} \cdot \nabla)\boldsymbol{V} \\ (m_4, m_5, m_6) &= -(\boldsymbol{n} \cdot \nabla)(\boldsymbol{r} \times \boldsymbol{V}) \\ \boldsymbol{r} &= (x, y, z) \\ \boldsymbol{V} &= \nabla \Phi_B = \nabla[-x + \phi_S(x, y, z)] \end{aligned}\right\}. \tag{3}$$

Here, S_H denotes the mean wetted surface of the ship hull, $\boldsymbol{n}$ is the normal vector defined as positive when pointing into the fluid region from the boundary surface, $\boldsymbol{r}$ is the position vector, and $\boldsymbol{V}$ is the velocity vector of steady flow induced by the double-body velocity potential Φ_B.

The linearized free-surface boundary condition to be satisfied by the radiation potential ϕ_j is written as follows:

$$\begin{aligned} &-g\frac{\partial \phi_j}{\partial z} + (i\omega)^2 \phi_j + 2i\omega\, U \overline{\nabla} \Phi_B \cdot \overline{\nabla} \phi_j \\ &\quad + U^2 \overline{\nabla} \Phi_B \cdot \overline{\nabla} \left(\overline{\nabla} \Phi_B \cdot \overline{\nabla} \phi_j \right) + \frac{1}{2} U^2 \overline{\nabla} \left(\overline{\nabla} \Phi_B \cdot \overline{\nabla} \Phi_B \right) \cdot \overline{\nabla} \phi_j \\ &\quad + \left(U \overline{\nabla}^2 \Phi_B + \mu \right) \left(i\omega + U \overline{\nabla} \Phi_B \cdot \overline{\nabla} \right) \phi_j = 0 \quad \text{on } z = 0, \end{aligned} \tag{4}$$

where g is the acceleration due to gravity, $\overline{\nabla}$ denotes the gradient operator only in the horizontal plane (x, y), and μ is Rayleigh's artificial viscosity coefficient ensuring the radiation condition be satisfied at infinity.

2.2. Note on the slender ship theory

The aforementioned 3D boundary value problem may be solved with a sophisticated numerical solution method like RPM. However, it is of engineering importance to consider a simplified and fast computation method while keeping sufficient accuracy and making it easier to understand hydrodynamic implication and importance of each term in the boundary conditions. It may be possible for slender ships by introducing the slenderness parameter ϵ as a guide, which is usually taken as B/L or d/L, with B, d, L being ship's breadth, draft, and length, respectively. In the limit of $\epsilon \to 0$, the ship will be viewed as a segment in the x-axis, and then the body boundary condition cannot be imposed, but the 3D wave pattern is important on the free surface (which is called the outer problem). On the other hand, in the near field close to the body surface, the y- and z-axes may be stretched by the variable transformation of $y = \epsilon Y$ and $z = \epsilon Z$. Then, the body boundary condition can be satisfied in the magnified Y-Z plane. On the contrary, however, a proper behavior of outgoing waves cannot be detected in the inner problem, and hence, no radiation condition is imposed. In this inner problem, the free-surface boundary condition may be simplified depending on the order of oscillation frequency ω and forward speed U relative to the rate of change of the velocity potential in the transverse and longitudinal directions. To assume the orders of ω and U are equivalent to consider the relative length of the waves generated by the harmonic oscillation $2\pi g/\omega^2$ and the steady translation $2\pi U^2/g$, respectively, although the entire wave pattern of real 3D waves changes with ω and U (Becker 1958).

In both outer and inner problems, a unique solution cannot be obtained because of the lack of certain boundary condition, and hence, a homogeneous solution may be allowed in each problem. The unknown coefficients of these homogeneous components will be determined later through matching between outer and inner solutions in an overlap region.

Before describing details of the outer and inner solutions, let us focus our attention on the free-surface condition by assuming the relative orders of ω and U in terms of the slenderness parameter ϵ. For brevity of explanation, we adopt the uniform flow approximation for the steady velocity potential $\Phi_B \simeq -x$ and omit Rayleigh's artificial viscosity μ in equation (4). Then, the free-surface boundary condition takes the following form:

$$\frac{\partial \phi_j}{\partial z} - \frac{1}{g}\left(i\omega - U\frac{\partial}{\partial x} \right)^2 \phi_j = 0 \quad \text{on } z = 0. \tag{5}$$

This is valid in the outer field far from the ship and represents 3D wave systems changing with ω and U.

For convenience in subsequent analyses, the Fourier transform with respect to x will be used with the following definition:

$$\left.\begin{aligned} F^*(k) &= \int_{-\infty}^{\infty} F(x) e^{ikx} dx \\ F(x) &= \frac{1}{2\pi} \int_{-\infty}^{\infty} F^*(k) e^{-ikx} dk \end{aligned}\right\}. \tag{6}$$

Because the Fourier transform of $\partial \phi_j / \partial x$ is given by $-ik\phi_j^*$, the Fourier transform of equation (5) with respect to x can be expressed as follows:

$$\frac{\partial \phi_j^*}{\partial z} + \kappa(k)\, \phi_j^* = 0 \quad \text{on } z = 0, \tag{7}$$

where

$$\kappa(k) = \frac{1}{g}(\omega + kU)^2 = K + 2\tau k + \frac{k^2}{K_0}, \tag{8}$$

$$K = \frac{\omega^2}{g},\ \tau = \frac{U\omega}{g},\ K_0 = \frac{g}{U^2}. \tag{9}$$

We note that $\kappa(k)$ defined by equation (8) is the 3D wave number including both ω and U and that appearance of the Fourier transform variable k implies the 3D effect, and at the same time, the forward-speed effect related to differentiation with respect to x multiplied by U.

Like conventional strip theories, by assuming the orders of ω and U as $\omega = O(\epsilon^{-1/2})$ and $U = O(1)$, the relative order of each term in equation (7) can be evaluated in the inner region of $z = O(\epsilon)$ given as follows:

$$\frac{\partial \phi_j^*}{\partial z} + K\phi_j^* + 2\tau k\phi_j^* + \frac{k^2}{K_0}\phi_j^* = 0 \quad \text{on } z = 0. \tag{10}$$

$$O(1) \quad O(1) \quad O(\sqrt{\epsilon}) \quad O(\epsilon)$$

Therefore, we can see that the leading term equation comprises the first two terms and can be written as follows:

$$\frac{\partial \phi_j^*}{\partial z} + K\phi_j^* = 0 \quad \text{on } z = 0, \tag{11}$$

which is the boundary condition for $k = 0$, namely, for the 2D and zero-speed case.

It has been argued that the strip theory satisfying equation (11) is valid only in a high-frequency range of $\omega = O(\epsilon^{-1/2})$, which is not true. As long as $U = 0$, equation (11) is valid even for low frequencies including the limit of $\omega \to 0$. However, because the third and fourth terms in equation (10) are neglected as higher orders from the outset, the forward-speed effect in the free-surface condition cannot be incorporated in the strip theory solution, no matter how we manipulate. In fact, for the forward-speed case, if we would consider $\omega = O(1)$ or $O(\epsilon)$, the third and fourth terms become of leading order, and hence, not only the second term but also the third and fourth terms should be taken into account in some way. We should emphasize that the difference in the order of the third term from the leading term is simply $O(\sqrt{\epsilon})$ even in the high-frequency regime.

One smart method for taking account of 3D and forward-speed effects (i.e., the terms including variable k) in equation (10) in the framework of 2D solution is the UT by Newman (1978). As will be shown later, those effects included in the outer solution typically expressed with a 3D wave number $\kappa(k)$ are incorporated into the inner solution through the coefficient of homogeneous component, which could be realized by matching with the outer solution at lower frequencies. Hence, the homogeneous coefficient is given as a function of k and 3D wave number $\kappa(k)$. However, the free-surface condition satisfied by the particular and homogeneous solutions remains equation (11). Probably, because of this treatment for the forward-speed effects, computed results by the UT for cross-coupling radiation forces between heave and pitch are not in good agreement with measured results (Kashiwagi et al. 2000). Nevertheless, effectiveness of including a homogeneous component in the inner solution to account for 3D effects prominent at low frequencies can be well recognized from an article of Kashiwagi and Ohkusu (1991) on tank wall interference effects on an oscillating ship with forward speed.

Another smart method for taking account of the forward-speed effect in the free-surface condition under the assumption of $\omega = O(\epsilon^{-1/2})$ and $U = O(1)$ is the RST by Ogilvie and Tuck (1969). To incorporate the third term proportional to τ in equation (10) into the particular solution of the inner problem, they adopted a systematic perturbation analysis and expressed the unsteady velocity potential in a power series of increasing order $\sqrt{\epsilon}$ as follows:

$$\phi_j^* = \phi_j^{(1)} + \sqrt{\epsilon}\,\phi_j^{(2)} + \cdots. \tag{12}$$

Then, the leading order forward-speed correction in equation (10) was considered in the following perturbation procedure:

$$\left.\begin{aligned} \frac{\partial \phi_j^{(1)}}{\partial z} + K\phi_j^{(1)} = 0 \quad \text{on } z = 0 \\ \frac{\partial \phi_j^{(2)}}{\partial z} + K\phi_j^{(2)} = -2\tau k\phi_j^{(1)} \quad \text{on } z = 0 \end{aligned}\right\}. \tag{13}$$

Exactly speaking, as will be shown later, there exist some other nonhomogeneous terms to be included on the right-hand side for $\phi_j^{(2)}$ which are contributions from interactions between the steady perturbation and unsteady flows and are the same order proportional to τ in a systematic analysis with slender ship assumption.

Because the left-hand side of equation (13) is the same as equation (11), the solution method for satisfying equation (13) can be essentially the same as that for the 2D problems. Although the analysis for $\phi_j^{(2)}$ in the RST is rather complicated, the final results for computing hydrodynamic forces are simple, contributing only to the cross-coupling terms in proportion to τ, and can be computed only with information of the leading term $\phi_j^{(1)}$ in equation (13). However, unlike the UT, no homogeneous component is allowed in the inner solution. Thus, in a low-frequency range where the second and third terms become smaller in order than the fourth term in equation (10), the analysis of the RST may be invalid, despite a fact that there are no numerical difficulties even when ω and U become small.

To circumvent the aforementioned deficiencies in the UT and RST, we should consider a hybrid method combining important ideas in both UT and RST, namely, the RST analysis will be used to incorporate the forward-speed effect (proportional to τ) of the free-surface condition into the particular inner solution, and the idea of the UT will be used to incorporate 3D and forward-speed effects (which become important in a low-frequency range) into the coefficient of homogeneous inner solution through matching with the outer solution. This hybrid analysis method in the framework of the slender ship theory is newly proposed in this article and notable in that the free-surface forward-speed effect proportional to τ can be taken into account in the inner particular solution, and other 3D and forward-speed effects can be incorporated in the inner homogeneous solution.

One may say that satisfaction of the free-surface condition with 3D wave number $\kappa(k)$ kept in equation (7) is possible within the 2D Laplace equation by using a numerical solution method like the 2D + T theory (Chapman 1976; Yeung & Kim 1981; Faltinsen & Zhao 1991, to name a few). However, computation methods for that formulation are much more complicated and time-consuming than the strip theory-type solution method. Hence, if we would seek a solution satisfying the 3D forward-speed free-surface condition, it may be better to use a fully 3D numerical solution method like RPM, rather than the 2D + T theory. The method newly proposed in this study keeps the framework of the 2D strip theory for an engineering purpose and improves the EUT, particularly in the accuracy of cross-coupling radiation forces due to the free-surface forward-speed effect proportional to $\tau = U\omega/g$.

2.3. Outer solution and its expansion

In the outer region far from the ship, the steady disturbance described by ϕ_S decays, and thus an approximation of $\Phi_B \simeq -x$ is acceptable. In this case, the free-surface boundary condition, equation (4), can be simplified as equation (5). The velocity

potential of hydrodynamic point source with unit strength satisfying equation (5) together with a proper radiation condition and 3D Laplace's equation is known as the 3D Green function (which will be subsequently denoted as G_{3D}). Because the ship may be viewed as a segment along the x-axis in the outer region, the outer solution can be described by a line distribution of 3D sources, in the form given as follows:

$$\begin{aligned}\phi_j^{(o)}(x,y,z) &= \int_{-\infty}^{\infty} Q_j(\xi) G_{3D}(x-\xi,y,z)\,d\xi \\ &= \frac{1}{2\pi}\int_{-\infty}^{\infty} Q_j^*(k) G_{3D}^*(k;y,z) e^{-ikx}\,dk,\end{aligned} \tag{14}$$

where Q_j is the unknown source strength along the x-axis, and thus, the outer solution expressed by equation (14) is the so-called homogeneous solution. The asterisk in the superscript in equation (14) stands for the Fourier transform with respect to x, defined by equation (6).

The Fourier transform of the 3D Green function has been well studied. Referring to the result in Kashiwagi (1997), its expansions at higher and lower frequencies may be expressed as follows:

$$\begin{aligned}G_{3D}^*(k;y,z) &\sim i\epsilon_k\, e^{-\kappa(k)(z+i\epsilon_k|y|)} \\ &\simeq \mathrm{i}e^{-K(z+i|y|)}\{1-2\tau k(z+i|y|)\} \\ &\quad + O\big((\kappa R)^{-1},\, k^2/\kappa^2\big) \quad \text{for } KR \gg 1,\end{aligned} \tag{15}$$

$$\begin{aligned}G_{3D}^*(k;y,z) &\sim G_{2D}(y,z) - \frac{1}{\pi}(1-Kz) f^*(k) \\ &\quad + O\big(K^2R^2,\, (\kappa-K)R,\, k^2R^2\big) \quad \text{for } KR \ll 1,\end{aligned} \tag{16}$$

where $R=\sqrt{y^2+z^2}$ and the 3D wave number $\kappa(k)$ is defined in equation (8). The symbol ϵ_k is defined as $\epsilon_k = \mathrm{sgn}(\omega + kU)$, which is equal to 1.0 at higher frequencies. Function $f^*(k)$ in equation (16) accounts for 3D and forward-speed effects in a low-frequency range, which is given by the following equation:

$$\begin{aligned}f^*(k) &= \ln\frac{2K}{|k|} + \pi i \\ &\quad - \begin{bmatrix} \dfrac{\kappa}{\sqrt{\kappa^2-k^2}}\left\{\pi i\epsilon_k + \cosh^{-1}\left(\dfrac{\kappa}{|k|}\right)\right\} \\ \dfrac{\kappa}{\sqrt{k^2-\kappa^2}}\left\{-\pi + \cos^{-1}\left(\dfrac{\kappa}{|k|}\right)\right\} \end{bmatrix},\end{aligned} \tag{17}$$

where the upper and lower expressions in the brackets apply to $\kappa > |k|$ and $\kappa < |k|$, respectively.

We note that equation (15) includes the leading two different orders under the assumption of $\omega = O(\epsilon^{-1/2})$ and $U = O(1)$, adopted in the RST, which is obtained by taking the first two terms in the expansion of $\kappa(k)$ shown in equation (8). In the original EUT, an approximation of $\kappa(k) \simeq K$ is used in equation (15). We also note that $G_{2D}(y,z) = G_{3D}^*(0;y,z)$ in equation (16). All terms containing valuable k are related to the x-dependency (i.e., 3D effects) through the Fourier transform. It is worth mentioning that the 3D wave number $\kappa(k)$ is kept in equation (17) without any simplification.

Substituting these results in equation (14) and using some formulae in the inverse Fourier transform, we can obtain the expansion of the outer solution, necessary for matching with the inner solution in an overlap region, in the form given as follows:

$$\begin{aligned}&\phi_j^{(o)}(x,y,z) \simeq \mathrm{i}e^{-K(z+i|y|)}\left\{Q_j(x) - i2\tau(z+i|y|)Q_j'(x)\right\} \\ &\quad \text{for } KR \gg 1,\end{aligned} \tag{18}$$

$$\begin{aligned}&\phi_j^{(o)}(x,y,z) \simeq Q_j(x) G_{2D}(y,z) \\ &\quad -\frac{1}{\pi}(1-Kz)\int_{-\infty}^{\infty} Q_j(\xi) f(x-\xi)\,d\xi \quad \text{for } KR \ll 1.\end{aligned} \tag{19}$$

Detailed expression for the kernel function $f(x-\xi)$ in equation (19), used in numerical computations, can be found in Newman and Sclavounos (1980).

2.4. Inner solution and its expansion

In the inner region close to the ship hull, the governing equation for the velocity potential can be the 2D Laplace equation because of variable stretching in the y- and z-axes with the slenderness parameter ϵ. Furthermore, from the body boundary condition, the order of ϕ_S for the steady disturbance flow can be estimated as ϵ^2. Then, under the assumption of $\omega = O(\epsilon^{-1/2})$ and $U = O(1)$ as in the RST, the two-term expansion of the body and free-surface boundary conditions given by equations (2–4) may take the following form:

$$[H]\frac{\partial\phi_j}{\partial n} = N_j + \frac{U}{i\omega}M_j \quad \text{on } S_H(x), \tag{20}$$

$$[F]\frac{\partial\phi_j}{\partial z} + K\phi_j = -\frac{i\omega U}{g}\left\{2\frac{\partial\phi_j}{\partial x} - 2\frac{\partial\phi_S}{\partial y}\frac{\partial\phi_j}{\partial y} - \frac{\partial^2\phi_S}{\partial y^2}\phi_j\right\} \quad \text{on } z=0, \tag{21}$$

where N_j and M_j are slender body approximations of n_j and m_j defined in equation (3), and the order of magnitude of both terms is the same and $O(\epsilon)$ for $j = 1$ and $O(1)$ for $j = 3$ and 5. Therefore, with assumption of $\omega = O(\epsilon^{-1/2})$ and $U = O(1)$, the speed-dependent terms proportional to U in both equations (20) and (21) are smaller than the zero-speed leading terms, with relative difference in the order of $\sqrt{\epsilon}$, namely, the radiation potential ϕ_j is expected to be a power series of increasing order $\sqrt{\epsilon}$, with the leading term being of zero-speed case and its order being $\phi_1 = O(\epsilon^2)$, $\phi_3 = O(\epsilon)$, and $\phi_5 = O(\epsilon)$.

By taking account of this order estimation and the knowledge learned from the UT (Newman 1978) regarding the existence of a homogeneous solution in the case of no radiation condition, we can construct the inner solution in the following form:

$$\phi_j^{(i)}(x;y,z) = \varphi_j(y,z) + C_j(x)\varphi_H(y,z) + \frac{U}{i\omega}\left\{\hat{\varphi}_j(y,z) + (i\omega)^2\psi_j(y,z)\right\}, \tag{22}$$

where φ_j and $\hat{\varphi}_j$ are the particular solutions satisfying the following boundary conditions:

$$\left.\begin{aligned}\frac{\partial\varphi_j}{\partial n} &= N_j \quad \text{on } S_H(x) \\ \frac{\partial\varphi_j}{\partial z} + K\varphi_j &= 0 \quad \text{on } z=0\end{aligned}\right\}, \tag{23}$$

$$\left.\begin{aligned}\frac{\partial\hat{\varphi}_j}{\partial n}&=M_j \quad \text{on } S_H(x)\\ \frac{\partial\hat{\varphi}_j}{\partial z}+K\hat{\varphi}_j&=0 \quad \text{on } z=0\end{aligned}\right\}. \tag{24}$$

$\varphi_H(y, z)$ in equation (22) is a homogeneous solution which is permitted in the inner problem because of no radiation condition. The solution satisfying homogeneous body and free-surface boundary conditions can be obtained as $\varphi_H(y,z)=\varphi_3(y,z)-\overline{\varphi_3(y,z)}$, where the overbar denotes the complex conjugate, and $C_j(x)$ in equation (22) is the coefficient of homogeneous solution which is unknown at this stage and to be determined from matching. The last term $\psi_j(y, z)$ in equation (22) is supplemented to account for the forward-speed effect on the right-hand side of the free-surface condition given by equation (21).

Taking the same order terms after substituting equation (22) into equations (20) and (21), the body and free-surface conditions for the supplementary term ψ_j can be of the following form:

$$\left.\begin{aligned}\frac{\partial\psi_j}{\partial n}&=0 \quad \text{on } S_H(x)\\ \frac{\partial\psi_j}{\partial z}+K\psi_j&=\\ -\frac{1}{g}\left\{2\frac{\partial\varphi_j}{\partial x}-2\frac{\partial\phi_S}{\partial y}\frac{\partial\varphi_j}{\partial y}-\frac{\partial^2\phi_S}{\partial y^2}\varphi_j\right\}&\text{ on } z=0\end{aligned}\right\}. \tag{25}$$

We note that the order of ψ_j must be the same as $\epsilon\times O(\varphi_j)$, i.e., $\psi_j=O(\epsilon^2)$ for $j=3$ and 5; thus, $(i\omega)^2\psi_j$ in equation (22) is of $O(\epsilon)$, which is the same as that of $\hat{\varphi}_j$.

For matching with the outer solution in an overlap region, let us consider an asymptotic expression of equation (22) at a far field for larger values of KR. Because evanescent waves may be neglected, the following results can be readily obtained:

$$\left.\begin{aligned}\varphi_j&\sim i\sigma_j(x)e^{-K(z+i|y|)}\\ \hat{\varphi}_j&\sim i\hat{\sigma}_j(x)e^{-K(z+i|y|)}\end{aligned}\right\}, \tag{26}$$

where $\sigma_j(x)$ and $\hat{\sigma}_j(x)$ are the 2D Kochin functions computed from φ_j and $\hat{\varphi}_j$, respectively. Specifically, they can be computed as follows:

$$\sigma_j(x)=\int_{S_H(x)}\left(\frac{\partial\varphi_j}{\partial n}-\varphi_j\frac{\partial}{\partial n}\right)e^{-Kz+iKy}d\ell \tag{27}$$

$$\hat{\sigma}_j(x)=\int_{S_H(x)}\left(\frac{\partial\hat{\varphi}_j}{\partial n}-\hat{\varphi}_j\frac{\partial}{\partial n}\right)e^{-Kz+iKy}d\ell \tag{28}$$

The inhomogeneous free-surface condition for ψ_j shown in equation (25) implies that the flow is the same as that induced by the following pressure distribution on the free surface

$$\begin{aligned}P(x;y)&=-\frac{\rho}{i\omega}\left\{2\frac{\partial\varphi_j}{\partial x}-2\frac{\partial\phi_S}{\partial y}\frac{\partial\varphi_j}{\partial y}-\frac{\partial^2\phi_S}{\partial y^2}\varphi_j\right\}_{z=0}\\ &\sim-\frac{2\rho}{\omega}\sigma_j'(x)e^{-iK|y|}+p_F(x;y),\end{aligned} \tag{29}$$

where $p_F(x; y)$ represents a regular pressure distribution due to the decaying behavior of ϕ_S as $|y|\to\infty$.

Using the analysis in terms of the Fourier transform and neglecting evanescent-wave terms, the asymptotic expression for ψ_j originating from the first term on the right-hand side of equation (29) takes the form as follows:

$$\begin{aligned}\psi_j(y,z)&=-\frac{2}{g\pi}\sigma_j'(x)\lim_{\mu\to0}\int_{-\infty}^{\infty}\frac{Ke^{-|m|z+imy}}{(m^2-K^2)(|m|-K+i\mu)}dm\\ &\sim-\frac{2}{g}i\sigma_j'(x)(z+i|y|)e^{-K(z+i|y|)}.\end{aligned} \tag{30}$$

Therefore, by collecting the results shown previously, the expansion of the inner solution valid for $KR\gg1$ can be obtained, which is essentially the same as that in the RST. On the other hand, the expansion for $KR\ll1$ can be the same as that in the UT. To sum up, the results of the inner solution expansion can be written as follows:

$$\phi_j^{(i)}(x;y,z)\simeq \mathrm{i}e^{-K(z+i|y|)}\left\{\sigma_j(x)+\frac{U}{i\omega}\hat{\sigma}_j(x)-i2\tau(z+i|y|)\sigma_j'(x)\right\}\quad \text{for } KR\ll1, \tag{31}$$

$$\phi_j^{(i)}(x;y,z)\simeq\left[\sigma_j(x)+\frac{U}{i\omega}\hat{\sigma}_j(x)+C_j(x)\left\{\sigma_3(x)-\overline{\sigma_3(x)}\right\}\right]G_{2D}(y,z)+i2C_j(x)\overline{\sigma_3(x)}e^{-Kz}\cos \mathrm{K}y\quad \text{for } KR\ll1. \tag{32}$$

By comparing these results with equations (18) and (19), we can realize that the matching for determining two unknowns, $Q_j(x)$ and $C_j(x)$, is possible, and the results are essentially the same as those in the UT (Kashiwagi 1997). The only difference is that the inner solution contains a new supplementary component $\psi_j(y, z)$ which represents a contribution from the speed-dependent convection term in the inner free-surface condition and is physically of critical importance as a correction to the UT. This term eventually contributes only to the cross-coupling added mass and damping coefficients as will be shown in the following section.

3. Hydrodynamic forces

3.1. Added mass and damping coefficients

Once the inner solution has been determined, the analyses for computing the hydrodynamic force can be a merger of both RST and UT. For the radiation problem, after applying the so-called Tuck's theorem (Ogilvie & Tuck 1969) to the integral of linearized pressure on the ship hull surface, the result can be expressed with the added mass (A_{jk}) and damping coefficient (B_{jk}) in the j-th direction because of the k-th mode of motion, in the form given as follows:

$$\begin{aligned}A_{jk}+\frac{1}{i\omega}B_{jk}&=-\rho\int_L dx\int_{S_H(x)}\left(N_j-\frac{U}{i\omega}M_j\right)\left\{\varphi_k+\frac{U}{i\omega}\hat{\varphi}_k\right\}d\ell\\ &\quad-\rho\int_L dxC_k(x)\int_{S_H(x)}\left(N_j-\frac{U}{i\omega}M_j\right)\left\{\varphi_3-\overline{\varphi_3}\right\}d\ell-\rho\, i2\tau\,\mathscr{Z}_{jk}.\end{aligned} \tag{33}$$

Here, $\mathscr{Z}_{jk}$ represents the additional term accounting for the forward-speed effect proportional to τ, to be computed from the

new term ψ_j (y, z) in the inner solution. Although the analytical transformation for this term is the same as shown in the study of Ogilvie and Tuck (1969), it is summarized in Appendix of this article for self-confirmation. From this transformation, we can see that $\mathscr{Z}_{jk} = 0$ for the case of $j = k$, and hence, the forward-speed effect in the free-surface condition contributes only to the cross-coupling terms of $j \neq k$. Specifically, the final result for the case of $j = 3$ and $k = 5$ (or $j = 5$ and $k = 3$) can be expressed as follows:

$$\left.\begin{aligned} \mathscr{Z}_{35} &= -\mathscr{Z}_{53} = \int_L I(x)dx \\ I(x) &= \int_{y_0(x)}^{\infty} \left\{\varphi_3^2(y,0) + \sigma_3^2 e^{-i2Ky}\right\}dy + \frac{i}{2K}\sigma_3^2\, e^{-i2Ky_0(x)} \end{aligned}\right\}, \tag{34}$$

where y_0 (x) denotes the half breadth of the transverse section S_H (x) at station x.

Once the solution of φ_3 for heave has been obtained, the 2D Kochin function σ_3 and the value of φ_3 $(y, 0)$ on the free surface necessary for computing equation (34) can be computed from the following expressions:

$$\sigma_3 = \int_{S_H(x)} \left(\frac{\partial \varphi_3}{\partial n} - \varphi_3 \frac{\partial}{\partial n}\right) e^{-K\zeta + iK\eta} d\ell\ , \tag{35}$$

$$\varphi_3(y,0) = \int_{S_H(x)} \left(\frac{\partial \varphi_3}{\partial n} - \varphi_3 \frac{\partial}{\partial n}\right) G_{2D}(y,0;\eta,\zeta) d\ell\ , \tag{36}$$

where $G_{2D}(y, z; \eta, \zeta)$ denotes the 2D free-surface Green function used in equations (16) and (32) and its computation method is well established.

It is noteworthy that the relation of $\mathscr{Z}_{35} = -\mathscr{Z}_{53}$ means that the Timman–Newman relation for the forward-speed effect (Timman & Newman 1962) is also satisfied in this additional term and that the analysis for the cross-coupling between sway ($j = 2$) and yaw ($j = 6$) can be performed in a similar manner.

In the slender ship analysis for the heave and pitch modes, we may approximate as $N_5 = -xN_3$, $M_5 = N_3$ for pitch. Thus, we have relations of $\varphi_5 = -x\varphi_3$, $\hat{\varphi}_5 = \varphi_3$ for the particular solutions and $\sigma_5 = -x\sigma_3$, $\hat{\sigma}_5 = \sigma_3$ for the 2D Kochin functions. The particular solution of the radiation potential φ_3 for an arbitrary 2D body shape can be obtained using the boundary element (or Green function) method.

3.2. Ship motions and added resistance

After computing hydrodynamic forces (not only in the radiation problem but also in the diffraction problem), the complex motion amplitude X_j ($j = 1, 3, 5$) can be obtained by solving the coupled motion equations of the form given as follows:

$$\sum_{k=1,3,5} \left[(i\omega)^2\left\{m_{jk}\delta_{jk} + A_{jk}\right\} + i\omega B_{jk} + C_{jk}\right] X_k = \zeta_a E_j \tag{37}$$

among the modes of surge ($j = 1$), heave ($j = 3$), and pitch ($j = 5$), where ζ_a denotes the amplitude of regular incident wave with circular frequency ω_0 (which is related to ω with $\omega = \omega_0 + U\omega_0^2/g$ in head wave), and E_j denotes the wave-exciting force in the j-th mode by the unit amplitude of incident wave. m_{jk} and δ_{jk} are the mass matrix coefficient and Kronecker's delta function, respectively; hence, m_{jk} is the ship's mass for $j = k = 1$ or 3, and the moment of inertia for $j = k = 5$. C_{jk} denotes the restoring force coefficient.

In terms of the complex motion amplitude computed, the 3D Kochin function for the term symmetric in the port and starboard sides can be computed from the linear superposition of the following form:

$$\left.\begin{aligned} H(k) &= H_7(k) - \frac{\omega\omega_0}{g}\sum_{j=1,3,5}\frac{X_j}{\zeta_a}H_j(k) \\ H_j(k) &= \int_L Q_j(\xi) e^{ik\xi} d\xi \end{aligned}\right\}, \tag{38}$$

where Q_j (x) is the strength of source distribution along the x-axis in the outer solution.

Once the 3D Kochin function could be computed, as well known as Maruo's formula (Maruo 1960), the added resistance in head waves can be computed from the following equation:

$$\begin{aligned} \frac{R_{AW}}{\rho g \zeta_a^2} &= \frac{1}{4\pi k_0}\left[-\int_{-\infty}^{k_1} + \int_{k_2}^{k_3} + \int_{k_4}^{\infty}\right]|H(k)|^2 \\ &\times \frac{\kappa}{\sqrt{\kappa^2 - k^2}}(k + k_0)dk. \end{aligned} \tag{39}$$

where

$$\left.\begin{matrix} k_1 \\ k_2 \end{matrix}\right\} = -\frac{K_0}{2}\left(1 + 2\tau \pm \sqrt{1 + 4\tau}\right), \tag{40}$$

$$\left.\begin{matrix} k_3 \\ k_4 \end{matrix}\right\} = \frac{K_0}{2}\left(1 - 2\tau \mp \sqrt{1 - 4\tau}\right). \tag{41}$$

We note that the wave numbers k_j ($j = 1 \sim 4$) are given as the roots of $\kappa^2 = k^2$; for $\tau > 1/4$, k_3 and k_4 become complex and the integration range in equation (39) must be continuous for $k_2 < k$; $k_0 = \omega_0^2/g$ is the wave number of incident wave in deep water; $\kappa(k)$ and $K_0 = g/U^2$ are defined in equations (8) and (9). There are a couple of points to be cautious in the numerical integration of equation (39), for which the readers are referred to Wicaksono and Kashiwagi (2018).

4. Results and discussion

To validate the present theory taking account of the forward-speed effect in the free-surface condition of the inner problem, computed results for the added mass and damping coefficients, particularly cross-coupling terms between heave and pitch, and also for the wave-induced ship motions (surge, heave, and pitch)

Table 1 Principal dimensions of a slender modified Wigley model

Length: L (m)	2.000
Breadth: B (m)	.300
Draft: d (m)	.125
Block coefficient: C_b	.5607
Displacement volume: $\nabla = C_b LBd$ (m^3)	.04205
Midship coefficient: C_m	.9091
Water-plane area: A_w (m^2)	.4160
Center of gravity: $\overline{OG}$ (m)	.0404
Gyrational radius: κ_{yy}/L	.248

in head waves are compared with corresponding values measured in the experiment.

The values to be computed by equation (33) may be divided into three components: the first term on the right-hand side is the same as the result of the strip method (which is referred to as New Strip Method (NSM) in subsequent comparisons), the second term on the right-hand side is the contribution from the homogeneous solution in the EUT (Kashiwagi 1997), and thus, the sum of the first and second terms is referred to as the EUT, and the third term is a newly added correction accounting for the forward-speed effect in the free-surface boundary condition in the inner problem. Therefore, the results including this correction term in the NSM and EUT are denoted as modified NSM (which is essentially the same as the RST) and modified EUT, respectively.

4.1. Slender modified Wigley model

The first comparison is made for a slender modified Wigley model, the geometry of which is expressed mathematically as follows:

$$y=\frac{B}{2}\left\{\left(1-\zeta^2\right)\left(1-\xi^2\right)\left(1+.2\xi^2\right)+\zeta^2\left(1-\zeta^8\right)\left(1-\xi^2\right)^4\right\}, \quad (42)$$

where $\xi = 2x/L$ and $\zeta = z/d$. The principal dimensions of this model used in the experiment by Kashiwagi et al. (2000) are shown in Table 1.

The cross-coupling added mass coefficients A_{53} and A_{35} (nondimensionalized with $\rho\nabla L$) and damping coefficients B_{53} and B_{35} (nondimensionalized with $\rho\nabla L\sqrt{g/L}$) are shown in Fig. 1 for $Fn = .2$, with abscissa taken as KL. As indicated in the legend, thin solid and dotted lines are the original EUT and NSM, respectively; thick solid and broken lines are the modified EUT and modified NSM, respectively, which contain the forward-speed correction term. We note that all these values in the cross-coupling terms are induced by the forward-speed effect only because the modified Wigley model considered is longitudinally symmetric, and hence, the values at zero forward speed must be exactly zero.

The agreement between the experiment and modified EUT is good enough over the range where experimental data are available, including the critical frequency $\tau = Fn\sqrt{KL} = .25$ (which corresponds to $KL = 1.56$ at $Fn = .2$). The modified NSM is also good in agreement, except in the very low-frequency range less than $\tau < .25$. We can see from these results that the additional term in the cross-coupling radiation forces, linearly proportional to the forward speed U and originating from the inner free-surface condition, is of critical importance for better agreement with experimental data in a low frequency range. Although the additional term ψ_j (y, z) in the inner solution of equation (22) is regarded as the second leading term under the assumption of $\omega = O(\epsilon^{-1/2})$ and $U = O(1)$; this term is the same in order as a particular solution $\hat{\varphi}_j(y,z)$ and computed with the leading-order solution φ_j (y, z), as shown in equations (25) and (34). Thus, as inferred from equations (22) and (33), the contribution from this additional term becomes practically important even in lower frequencies as a forward-speed effect proportional to τ originating from the free-surface condition. In a low-frequency range, other

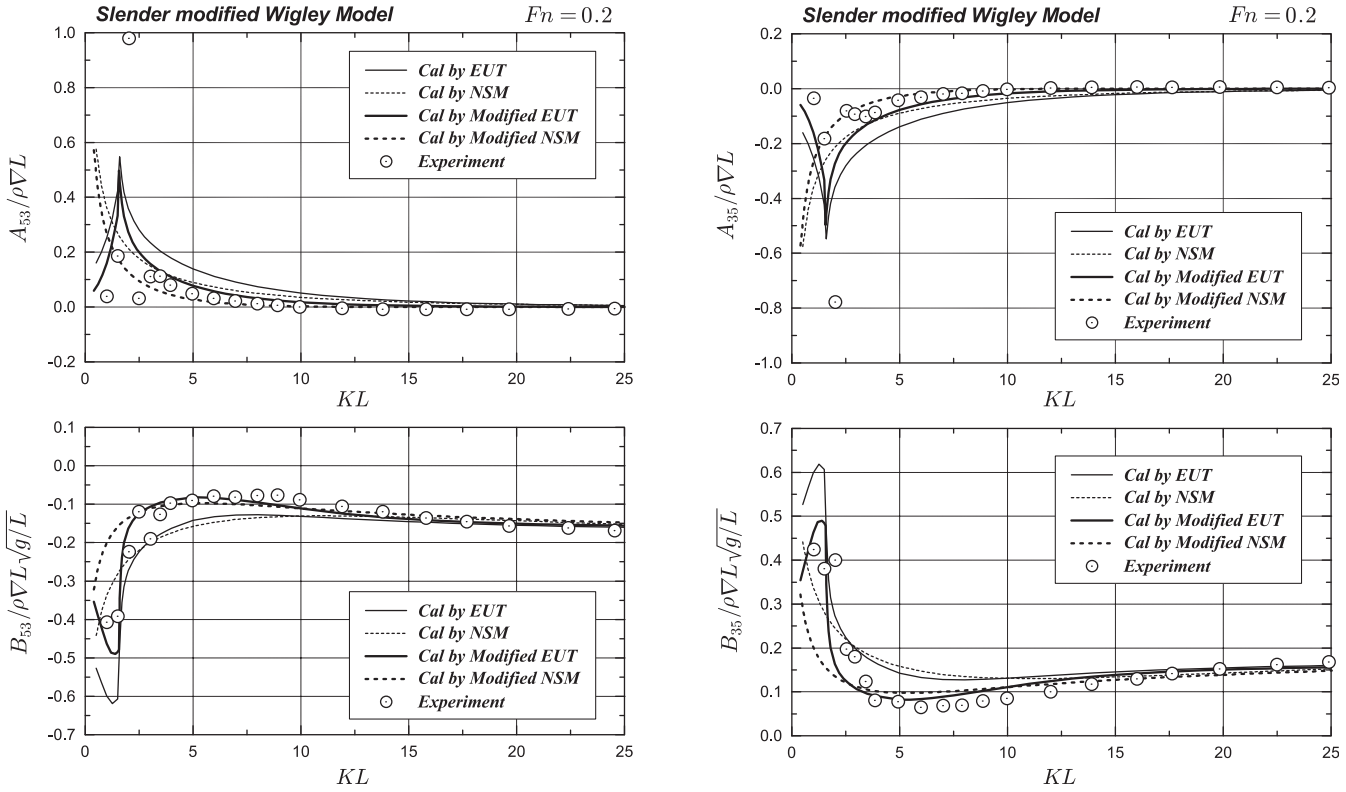

Fig. 1 Cross-coupling added mass and damping coefficients between heave and pitch for a slender modified Wigley model, at Fn = .2

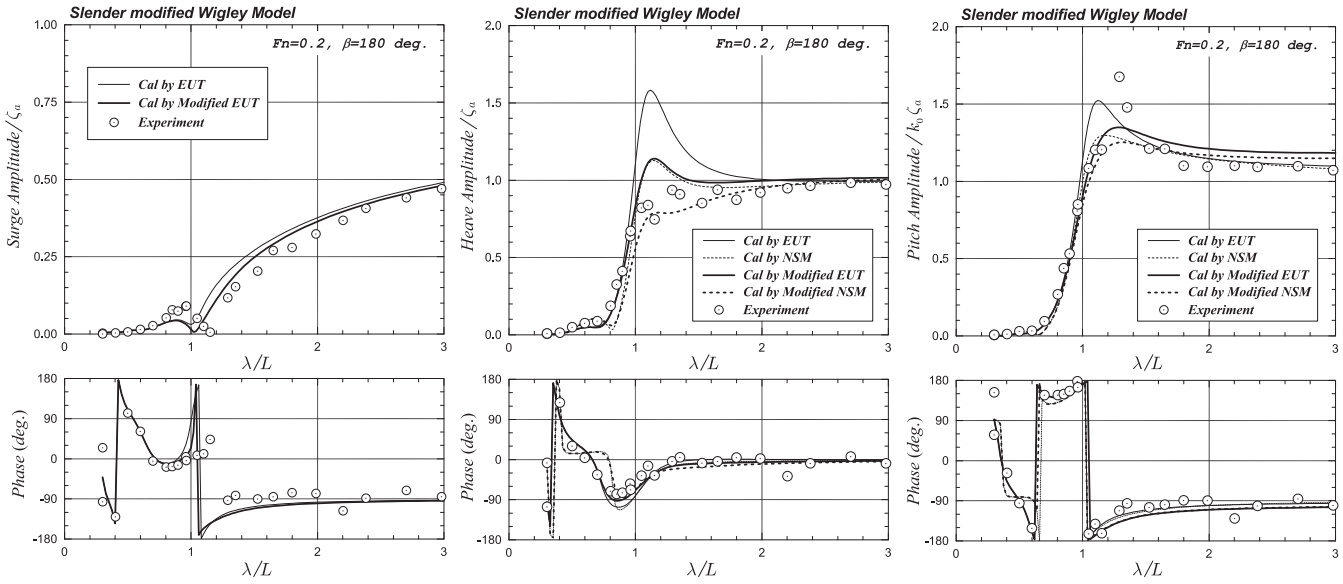

Fig. 2 Wave-induced ship motions (surge, heave, and pitch) of a slender modified Wigley model at Fn = .2 in head waves

forward-speed and 3D effects may become more important, which are taken into account through the homogeneous component of the inner solution.

Figure 2 shows the nondimensional amplitude and phase in surge, heave, and pitch motions. In the surge motion, only the results by the EUT are shown, and slight improvement can be observed by virtue of forward-speed correction in the heave–pitch coupling terms which is because the surge is computed from coupled motion equations among surge, heave, and pitch. More prominent improvement in agreement with the experiment can be observed in heave around a resonant frequency of $\lambda/L \simeq 1.1$. This prominent improvement indicates that the accuracy of cross-coupling added mass and damping coefficients between heave and pitch is of critical importance for predicting accurately the ship motions, particularly in heave, around the resonant frequency, because the diagonal components in the inertial force and restoring force coefficients almost cancel at the resonant frequency. In this case, the off-diagonal components become important, despite the magnitude of cross-coupling coefficients itself is relatively small as shown in Fig. 1. Similar observation regarding the importance of cross-coupling radiation forces around the motion-resonant wavelength was demonstrated experimentally in Kashiwagi et al. (2000).

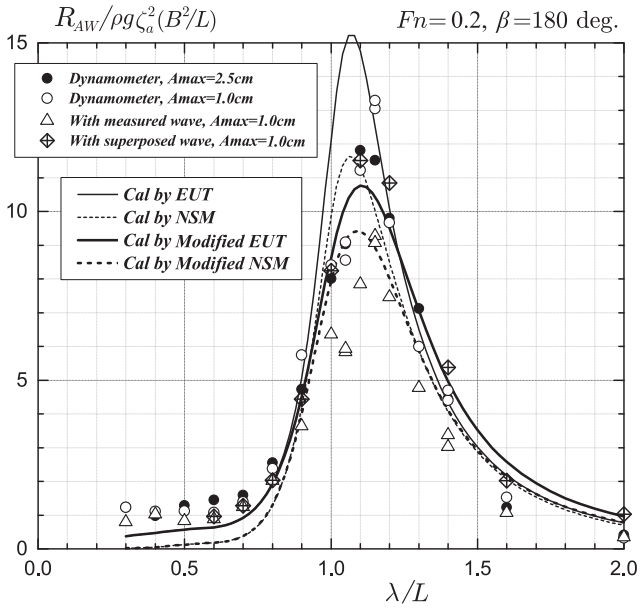

Fig. 3 Added resistance on a slender modified Wigley model at Fn = .2 in the motion-free condition in head waves

The added resistance computed with these complex motion amplitudes in surge, heave, and pitch is shown in Fig. 3, in which the experimental data for comparison are taken from Kashiwagi (2013). It can be seen that the prediction of added resistance, especially near its peak, is sensitive to a change in the complex motion amplitude, which is also the case in the experiment. By incorporating the linear forward-speed effect term in the heave–pitch cross-coupling radiation forces, the peak wavelength in the added resistance tends to shift slightly to a longer wavelength, agreeing with the experiment. However, the predicted values at longer wavelength region are obviously larger than the measured values, which may be attributed to overprediction of the pitch motion amplitude as observed in Fig. 2. A possible reason of this overprediction of the pitch motion is a slight discrepancy in the pitch damping coefficient and the pitch exciting moment as indicated in Kashiwagi et al. (2000), but more careful check should be made for confirming this conjecture.

4.2. RIOS bulk carrier

The RIOS at Osaka University provided a bulk carrier model which can be open to the public for experiments and numerical computations with research purpose. The principal dimensions of this model are shown in Table 2, and its body plan is also shown in Fig. 4.

Table 2 Principal dimensions of the RIOS bulk carrier model

Length between perpendiculars: L_{pp} (m)	2.400
Breadth: B (m)	.400
Draft: d (m)	.128
Block coefficient: C_b	.800
Displacement volume: $\nabla = C_b LBd\,(\mathrm{m}^3)$	.09830
Midship coefficient: C_m	.9950
Water-plane area: $A_w\,(\mathrm{m}^2)$	.8354
Center of gravity: $\overline{\mathrm{OG}}\,(\mathrm{m})$	.0205
Gyrational radius: κ_{yy}/L	.256

Measured and computed results for the cross-coupling added mass and damping coefficients between heave and pitch are shown in Fig. 5 in the same fashion as that for the slender modified Wigley model, but the Froude number in this comparison is $Fn = .18$. Clearly the degree of agreement is improved by adding the linear forward-speed correction term originating from the forward-speed effect in the inner free-surface condition. Around the critical frequency equal to $\tau = Fn\sqrt{KL} = .25$ ($KL = 1.93$ at $Fn = .18$), computed results show rapid change, which looks also observed in the experiment but a little exaggerated in the computation based on the linear potential flow theory.

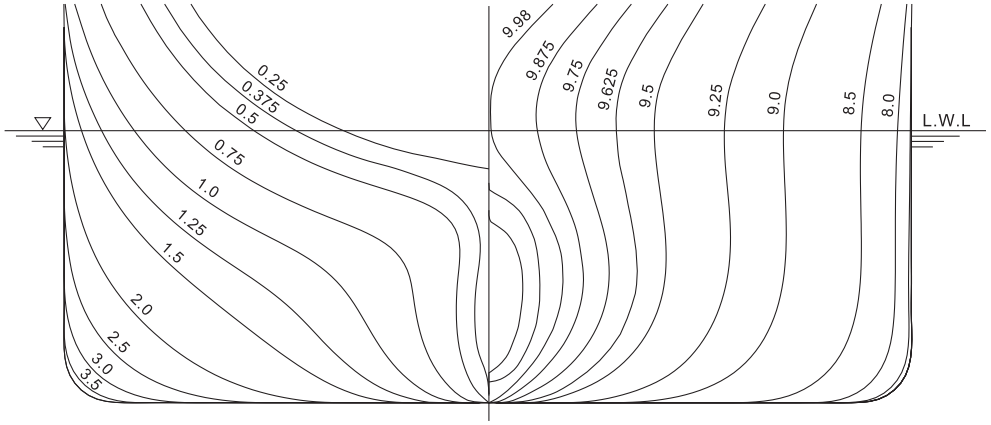

Fig. 4 Body plan of the RIOS bulk carrier

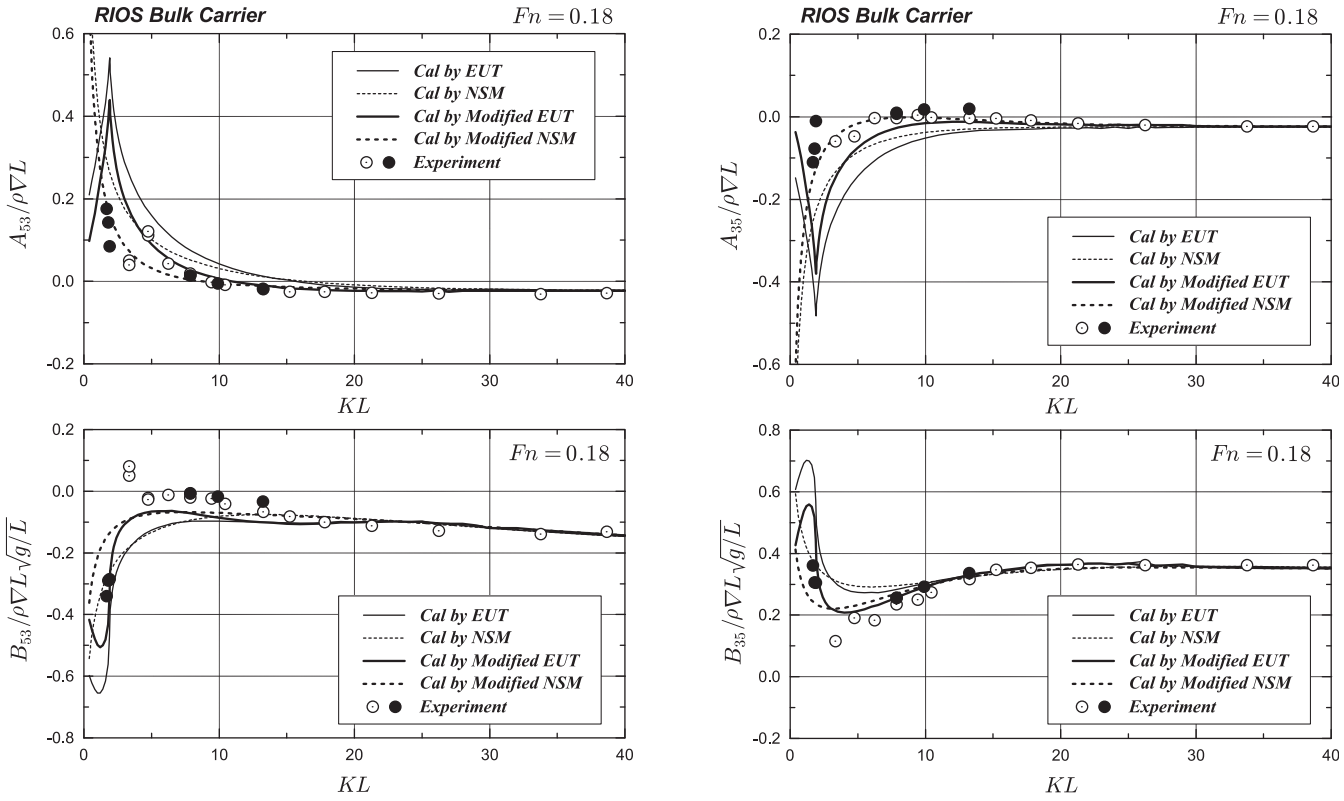

Fig. 5 Cross-coupling added mass and damping coefficients between heave and pitch for the RIOS bulk carrier model, at Fn = .18

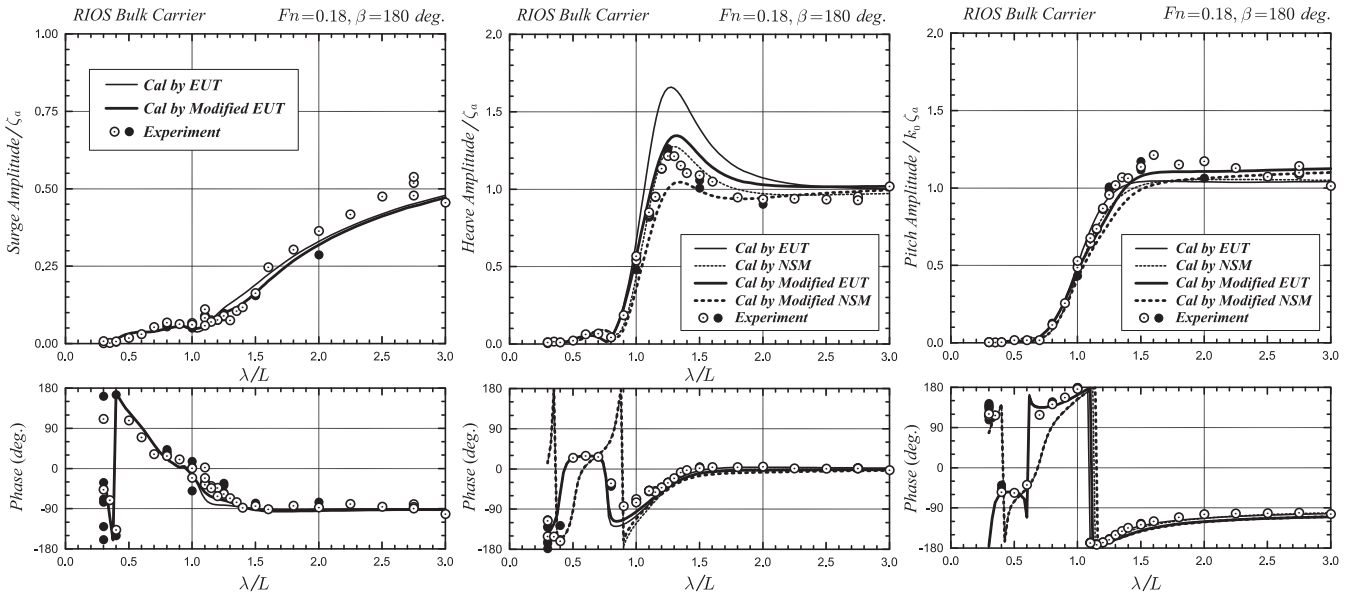

Fig. 6 Wave-induced ship motions (surge, heave, and pitch) of the RIOS bulk carrier model at Fn = .18 in head waves

Figure 6 shows the nondimensional amplitude and phase of wave-induced ship motions. We can see prominent improvement in the peak value of heave motion by the modified EUT taking account of the linear forward-speed effect term in the inner free-surface condition. We note that $\lambda/L = 1.25$ near the peak corresponds to $KL = 9.902$ at $Fn = .18$, where the improvement from the original EUT can be observed mainly in the added mass coefficients A_{53} and A_{35} rather than in the damping coefficients B_{53} and B_{35}. Therefore, we can say that the accuracy in the cross-coupling added mass coefficients is important for accurate prediction of the peak amplitude, especially in heave.

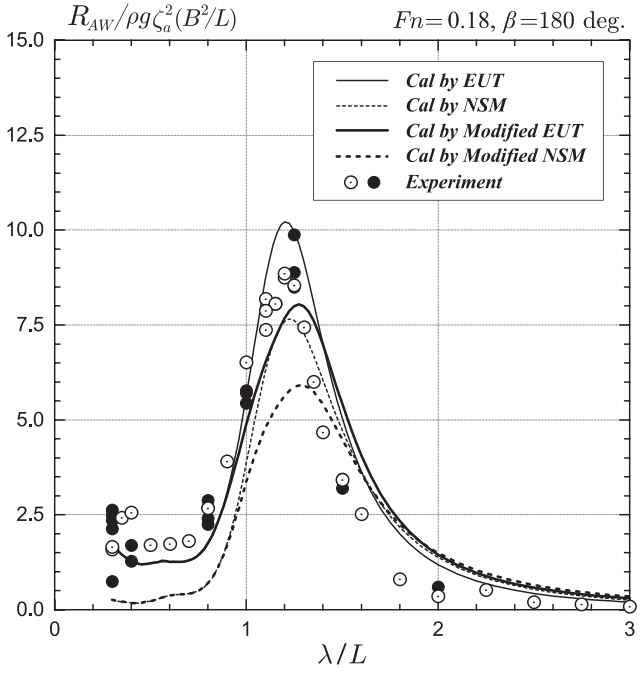

Fig. 7 Added resistance on the RIOS bulk carrier model at Fn = .18 in the motion-free condition in head waves

A comparison for the added resistance on the RIOS bulk carrier model is shown in Fig. 7. The degree of agreement between computed results by the modified EUT and measured results is unexpectedly not so good, and we can see again that the prediction of added resistance is sensitive to the complex amplitude of ship motions. The wavelength at which the added resistance takes the maximum looks slightly different in the modified EUT. (Note that $\lambda/L = 1.1$ and 1.2 correspond to $KL = 11.684$ and 10.437, respectively.) Looking at the pitch motion RAO in Fig. 6 and the added resistance in Fig. 7, we can conjecture that slight underprediction of pitch motion around $\lambda/L = 1.1 \sim 1.2$ may be a reason of the difference in the added resistance and slight overprediction of heave motion in the range of $\lambda/L > 1.25$ may be a reason of overprediction in the added resistance.

As we have seen, obviously the prediction accuracy is improved in the cross-coupling radiation forces and the resultant ship motions, especially in heave, but the prediction accuracy in the added resistance is not necessarily improved, especially for the RIOS bulk carrier model, which suggests that the total balance in computing the Kochin function would be important for accurate prediction of the added resistance.

5. Conclusions

Within the framework of the EUT, a study has been conducted on the effect of forward speed proportional to the parameter $\tau = U\omega/g$ in the inner free-surface condition on hydrodynamic radiation forces, wave-induced ship motions, and resultant added resistance. To compute the additional radiation forces originating from the term proportional to the forward speed of a ship in the inner free-surface condition, the solution method developed in Ogilvie and Tuck's RST has been adopted for the particular inner solution. The resultant contribution from this forward-speed effect exists only in the cross-coupling added mass and damping

coefficients, specifically between heave and pitch in the present study, which satisfies the Timman–Newman relation.

Numerical computations and comparison with measured results have been made for a slender modified Wigley model with longitudinal symmetry and a real ship of the RIOS bulk carrier with block coefficient $C_b = .8$. For both cases, prominent improvement in the cross-coupling added mass and damping coefficients between heave and pitch could be confirmed. Furthermore, it was confirmed that the improvement in these cross-coupling terms contributes to better agreement with measured results in the amplitude of ship motions (particularly in heave) near the resonant frequency. This is because the diagonal components in the inertial and restoring forces cancel, and hence, off-diagonal components become important at the resonant frequency.

However, the degree of improvement in the added resistance was found to be not so much as expected, and we realized that the prediction of added resistance is sensitive to slight change in the cross-coupling radiation forces and resultant ship motions, especially around the motion-resonant wavelength, because the added resistance takes the maximum near the motion-resonant wavelength. For more accurate prediction of the wave-making component in the added resistance, we should consider a computation method that is balanced in the degree of accuracy for computing the ship-generated wave-amplitude function known as the Kochin function over a wider range of wavelength.

Acknowledgments

A part of this study was supported by the JSPS Grant-in-Aid for Scientific Research (Grant number 17H01357) and also the subsidy for the International Collaboration Promotion Program at Osaka University, for which the author is thankful.

REFERENCES

Becker, E. 1958 Das Wellenbild einer unter der Oberfläche eines Stromes Schwerer Flüssigkeit pulsierender Quelle, *Zeitschrit Angewandte Mathematik and Mechanik*, **38**, 391–399.

Chapman, R. B. 1976 Free-surface effects for yawed surface-piercing plates, *Journal of Ship Research*, **20**(3), 125–136.

el Moctar, B. O., Sigmund, S., Ley, J., and Schellin, T. 2017 Numerical and experimental analysis of added resistance of ships in waves, *Journal of Offshore Mechanics and Arctic Engineering*, **139**(1), 001301.

Faltinsen, O. M. 1974 A numerical investigation of the Ogilvie-Tuck formulae for added-mass and damping coefficients, *Journal of Ship Research*, **18**(2), 73–84.

Faltinsen, O. M. and Zhao, R. 1991 Numerical predictions of ship motions at high forward speed, *Philosophical Transactions, Royal Society, Series A*, **334**(1634), 241–252.

ITTC Report of the Seakeeping Committee 2017 *Proceedings*, 28th ITTC, September 17–22, Wuxi, China, Vol. 1.

Kashiwagi, M. 1995 Prediction of surge and its effect on added resistance by means of the enhanced unified theory, *Transactions of the West-Japan Society of Naval Architects*, **89**, 77–89.

Kashiwagi, M. 1997 Numerical seakeeping calculations based on the slender ship theory, *Ship Technology Research (Schiffstechnik)*, **44**, 167–192.

Kashiwagi, M. 2009 Impact on hull design on the added resistance in waves–Application of the enhanced unified theory, , *Proceedings*, 10th International Marine Design Conference (IMDC), May 26–29, Trondheim, Norway, **Vol. 1**, 521–535.

Kashiwagi, M. 2013 Hydrodynamic study on added resistance using unsteady wave analysis, *Journal of Ship Research*, **57**(4), 220–240.

Kashiwagi, M., Kawasoe, K., and Inada, M. 2000 A study on ship motion and added resistance in waves, *Journal of Kansai Society of Naval Architects, Japan*, **234**, 85–94.

Kashiwagi, M. and Ohkusu, M. 1991 A new theory for side-wall interference effects on forward-speed radiation and diffraction forces, *Ship Technology Research (Schiffstechnik)*, **38**(1), 17–47.

Kim, M., Hizir, O., Turan, O., Day, S., and Incecik, A. 2017 Estimation of added resistance and ship speed loss in a seaway, *Ocean Engineering*, **141**, 465–476.

Kim, K. H. and Kim, Y. 2011 Numerical study on added resistance of ships by using a time-domain Rankine panel method, *Ocean Engineering*, **38**, 1357–1367.

Maruo, H. 1960 Wave resistance of a ship in regular head seas, *Bulletin of the Faculty of Engineering*, **9**, 73–91.

Minoura, M., Hanaki, T. and Nanjo, T. 2019 Improvement of statistical estimation of ship performance in actual seas by normalization of data unevenness using cluster analysis, *Proceedings*, 14th International Symposium on Practical Design of Ships and Other Floating Structures, September 22–26, Yokohama, Japan, PRADS2019-W4-C-1.

Newman, J. N. 1978 The theory of ship motions, *Advances in Applied Mechanics*, **18**, 221–283.

Newman, J. N., and Sclavounos, P. D. 1980 The unified theory of ship motions, *Proceedings*, 13th Symposium on Naval Hydrodynamics, October 6–10, Tokyo, Japan, 373–394.

Ogilvie, T. F. and Tuck, E. O. 1969 A rational strip theory of ship motions: Part 1, Report No. 13, Ann Arbor, Michigan: Naval Architecture and Marine Engineering, University of Michigan.

Orihara, H. and Tsujimoto, M. 2018 Performance prediction of full-scale ship and analysis by means of on-board monitoring. Part 2: Validation of full-scale performance, predictions in actual seas, *Journal of Marine Science and Technology*, **23**, (4), 782–801.

Sclavounos, P. D. 1984 The diffraction of free-surface waves by a slender ship, *Journal of Ship Research*, **28**(1), 29–47.

Shao, Y. L. and Faltinsen, O. M. 2012 Linear seakeeping and added resistance analysis by means of body-fixed coordinate system, *Journal of Marine Science and Technology*, **17**(4), 493–510.

Söding, H., Shigunov, V., Schellin, T. E., and el Moctar, O. 2014 A Rankine panel method for added resistance of ships in waves, *Journal of Offshore Mechanics and Arctic Engineering*, **136**(3), 031601.

Timman, R. and Newman, J. N. 1962 The coupled damping coefficients of a symmetric ship, *Journal of Ship Research*, **5**(4), 34–55.

Wicaksono, A. and Kashiwagi, M. 2018 Wave-induced steady forces and yaw moment of a ship advancing in oblique waves, *Journal of Marine Science and Technology*, **23**, 767–781.

Yeung, R. W. and Kim, S. H. 1981 Radiation forces on ships with forward speed, *Proceedings*, 3rd International Conference on Numerical Ship Hydrodynamics, June 16–19, Paris, France, 499–515.

Appendix analytical transformation for Z_{jk}

In terms of linearized Bernoulli's pressure equation, the hydrodynamic force can be computed and expressed as follows:

$$F_j = \sum_{k=1}^{6} T_{jk} X_k = \sum_{k=1}^{6} \left[-(i\omega)^2 \left\{ A_{jk} + \frac{1}{i\omega} B_{jk} \right\} \right] X_k. \tag{A1}$$

Here, T_{jk} is referred to as the transfer function for the force acting in the j-th direction due to the k-th mode of motion, and the contribution from the velocity potential ψ_k in equation (22) to the transfer function may be computed from the following equation:

$$T_{jk}^{(2)} \equiv \rho (i\omega)^3 U \int_L \mathrm{dx} \int_{S_H(x)} \psi_k N_j d\ell \,. \tag{A2}$$

Thus, we will consider the following integral along the sectional contour at station x.

$$I_{jk}(x) \equiv \int_{S_H(x)} \psi_k N_j d\ell \,. \tag{A3}$$

Taking account of the body boundary conditions for ψ_k and φ_j and applying Green's theorem, we have the following equation:

$$I_{jk}=\int_{S_H(x)}\left\{\psi_k\frac{\partial\varphi_j}{\partial n}-\varphi_j\frac{\partial\psi_k}{\partial n}\right\}d\ell=-\left[\int_{C_F}+\int_{C_\infty}\right]\left\{\psi_k\frac{\partial\varphi_j}{\partial n}-\varphi_j\frac{\partial\psi_k}{\partial n}\right\}d\ell \tag{A4}$$

On the free surface (C_F), $d\ell=-dy$ and $\partial/\partial n=\partial/\partial z$. Hence, from the free-surface boundary conditions for ψ_k and φ_j, it follows the following equation:

$$\begin{aligned}\mathscr{J}_F&\equiv-\int_{C_F}\left\{\psi_k\frac{\partial\varphi_j}{\partial n}-\varphi_j\frac{\partial\psi_k}{\partial n}\right\}d\ell\\&=-\frac{2}{g}\int_{y_0(x)}^{\infty}\varphi_j\left\{2\frac{\partial\varphi_k}{\partial x}-2\frac{\partial\phi_S}{\partial y}\frac{\partial\varphi_k}{\partial y}-\frac{\partial^2\phi_S}{\partial y^2}\varphi_k\right\}dy,\end{aligned} \tag{A5}$$

where $y_0(x)$ denotes the half breadth of the transverse section $S_H(x)$ at station x.

Performing the partial integration for the last terms gives the following equation:

$$\begin{aligned}\mathscr{J}_F=&-\frac{4}{g}\int_{y_0(x)}^{\infty}\varphi_j\frac{\partial\varphi_k}{\partial x}dy\\&+\frac{2}{g}\int_{y_0(x)}^{\infty}\frac{\partial\phi_S}{\partial y}\left(\frac{\partial\varphi_k}{\partial y}\varphi_j-\varphi_k\frac{\partial\varphi_j}{\partial y}\right)dy\\&+\frac{2}{g}\left[\frac{\partial\phi_S}{\partial y}\varphi_j\varphi_k\right]_{y_0(x)}^{\infty}\end{aligned} \tag{A6}$$

Here, we note that the second term in equation (A6) becomes zero for $j=k$. Even for the case of $j\neq k$, this term can be found equal to zero for the coupling between heave ($j=3$) and pitch ($j=5$) because $\varphi_5=-x\varphi_3$ holds in the slender ship approximation.

To ensure the convergence in the integral with respect to y in the first term of equation (A6), the asymptotic expression of $\varphi_j\partial\varphi_k/\partial x$ will be subtracted from the integrand and added after analytical integration. Then, because the asymptotic expression of φ_j is given by equation (26), the result takes the following form:

$$\begin{aligned}\mathscr{J}_F=&-\frac{4}{g}\int_{y_0(x)}^{\infty}\left\{\varphi_j\frac{\partial\varphi_k}{\partial x}+\sigma_j\sigma_k^{'}e^{-i2Ky}\right\}dy\\&-\frac{2}{g}\left[\frac{\partial\phi_S}{\partial y}\varphi_j\varphi_k+\frac{i}{K}\sigma_j\sigma_k^{'}e^{-i2Ky}\right]_{y=y_0(x)}\\&+\frac{2i}{gK}\sigma_j\sigma_k^{'}\lim_{R\to\infty}e^{-i2KR}.\end{aligned} \tag{A7}$$

On the other hand, the line integral along C_∞ in equation (A4) (denoted as $\mathscr{J}_\infty$) can be evaluated analytically only with the asymptotic expressions given by equations (26) and (30). The result with this transformation can be written as follows:

$$\begin{aligned}\mathscr{J}_\infty&=2\int_0^{\infty}\left\{\psi_k\frac{\partial\varphi_j}{\partial y}-\varphi_j\frac{\partial\psi_k}{\partial y}\right\}_{y=\infty}dz\\&=-\frac{4i}{g}\sigma_j\sigma_k^{'}\lim_{y\to\infty}e^{-i2Ky}\int_0^{\infty}e^{-2Kz}dz.\end{aligned} \tag{A8}$$

We can see that this result exactly cancels out the last term in equation (A7) because the result of the integral with respect to z in equation (A8) is $1/2K$.

Because $I_{jk}(x)$ in equation (A4) is given by the sum of $\mathscr{J}_F$ and, $\mathscr{J}_\infty$ it follows the following form:

$$\begin{aligned}I_{jk}(x)=&-\frac{4}{g}\int_{y_0(x)}^{\infty}\left\{\varphi_j\frac{\partial\varphi_k}{\partial x}+\sigma_j\sigma_k^{'}e^{-i2Ky}\right\}dy\\&-\frac{2}{g}\left[\frac{\partial\phi_S}{\partial y}\varphi_j\varphi_k+\frac{i}{K}\sigma_j\sigma_k^{'}e^{-i2Ky}\right]_{y=y_0(x)}.\end{aligned} \tag{A9}$$

For further transformation, we will use the body boundary condition for the steady disturbance potential ϕ_S on $z=0$ given by the following equation:

$$\frac{\partial\phi_S}{\partial y}=-y_0^{'}(x)\quad\text{on } z=0 \tag{A10}$$

and the following identity:

$$\begin{aligned}&\frac{d}{dx}\int_{y_0(x)}^{\infty}\left\{\varphi_j\varphi_k+\sigma_j\sigma_k e^{-i2Ky}\right\}dy\\&=\int_{y_0(x)}^{\infty}\left\{\varphi_j\frac{\partial\varphi_k}{\partial x}+\sigma_j\sigma_k^{'}e^{-i2Ky}\right\}dy\\&+\int_{y_0(x)}^{\infty}\left\{\varphi_k\frac{\partial\varphi_j}{\partial x}+\sigma_k\sigma_j^{'}e^{-i2Ky}\right\}dy\\&-y_0^{'}(x)\left\{\varphi_j\varphi_k+\sigma_j\sigma_k e^{-i2Ky_0(x)}\right\}.\end{aligned} \tag{A11}$$

In the previous equation, we note that the left-hand side becomes zero after integrating it with respect to x over the ship's length, under the assumption that both ends of a ship smoothly close. With these equations, first we consider the case of $j=k$.

In this case, from equation (A11), we have the following equation:

$$\begin{aligned}&2\int_{y_0(x)}^{\infty}\left\{\varphi_j\frac{\partial\varphi_j}{\partial x}+\sigma_j\sigma_j^{'}e^{-i2Ky}\right\}dy\\&=y_0^{'}(x)\left\{\varphi_j^2+\sigma_j^2e^{-i2Ky_0(x)}\right\}.\end{aligned} \tag{A12}$$

Substituting this relation and equation (A10) into equation (A9), it follows the following equation:

$$\begin{aligned}I_{jj}(x)=&-\frac{2}{g}\left[y_0^{'}(x)\left\{\varphi_j^2+\sigma_j^2e^{-i2Ky_0(x)}\right\}\right.\\&\left.-y_0^{'}(x)\varphi_j^2+\frac{i}{K}\sigma_j\sigma_j^{'}e^{-i2Ky_0(x)}\right]\\=&-\frac{2}{g}\frac{d}{dx}\left[\frac{i}{2K}\sigma_j^2e^{-i2Ky_0(x)}\right].\end{aligned} \tag{A13}$$

Thus, this term becomes zero after integrating over the ship's length, with the same reason as for obtaining equation (A12). Therefore, we could prove that there is no component proportional to the forward speed in the diagonal added mass and damping coefficients.

Next, we consider the case of $j\neq k$, particularly the coupling between heave and pitch. In this case, approximations of $\varphi_5=-x\varphi_3$ and hence $\sigma_5=-x\sigma_3$ can be used in the slender ship theory. Thus, we can derive the following relation:

$$\varphi_3\frac{\partial\varphi_5}{\partial x}+\sigma_3\sigma_5^{'}e^{-i2Ky} = \varphi_5\frac{\partial\varphi_3}{\partial x}+\sigma_5\sigma_3^{'}e^{-i2Ky}-\left\{\varphi_3^2+\sigma_3^2e^{-i2Ky}\right\}. \tag{A14}$$

By applying this relation to equation (A11) for $(j,k)=(3,5)$ and $(j,k)=(5,3)$, we can obtain the following equation:

$$\begin{aligned}&\frac{d}{dx}\int_{y_0(x)}^{\infty}\left\{\varphi_j\varphi_k+\sigma_j\sigma_ke^{-i2Ky}\right\}dy\\&=2\int_{y_0(x)}^{\infty}\left\{\varphi_j\frac{\partial\varphi_k}{\partial x}+\sigma_j\sigma_k^{'}e^{-i2Ky}\right\}dy\\&\pm\int_{y_0(x)}^{\infty}\left\{\varphi_3^2+\sigma_3^2e^{-i2Ky}\right\}dy\\&-y_0^{'}(x)\left\{\varphi_j\varphi_k+\sigma_j\sigma_ke^{-i2Ky_0(x)}\right\},\end{aligned} \tag{A15}$$

where the upper (+) and lower (−) signs in the second line on the right-hand side of equation (A15) must apply to $(j,k)=(3,5)$ and $(j,k)=(5,3)$, respectively.

As before, the left-hand side of equation (A15) becomes zero after integration over the ship's length. With this kept in mind, we substitute equations (A10) and (A15) into equation (A9), then the result can be expressed as follows:

$$\begin{aligned}I_{jk}(x)=&\pm\frac{2}{g}\int_{y_0(x)}^{\infty}\left\{\varphi_3^2+\sigma_3^2e^{-i2Ky}\right\}dy\\&-\frac{2}{g}e^{-i2Ky_0(x)}\left\{\frac{i}{K}\sigma_j\sigma_k^{'}+y_0^{'}(x)\sigma_j\sigma_k\right\}.\end{aligned} \tag{A16}$$

Furthermore, we can prove the following relations:

$$\begin{aligned}&\frac{d}{dx}\left[\frac{i}{2K}\sigma_j\sigma_ke^{-i2Ky_0(x)}\right]\\&=e^{-i2Ky_0(x)}\left\{\frac{i}{K}\sigma_j\sigma_k^{'}+y_0^{'}(x)\sigma_j\sigma_k\right\}\\&+e^{-i2Ky_0(x)}\frac{i}{2K}\left(\sigma_j^{'}\sigma_k-\sigma_j\sigma_k^{'}\right),\end{aligned} \tag{A17}$$

$$\sigma_j^{'}\sigma_k-\sigma_j\sigma_k^{'}=\pm\sigma_3^2, \tag{A18}$$

where the meaning of the complex sign given earlier is the same as in equations (A15) and (A16). Substituting equations (A17) and (A18) in equation (A16), it follows the following form:

$$I_{jk}(x)=\pm\frac{2}{g}\left[\int_{y_0(x)}^{\infty}\left\{\varphi_3^2+\sigma_3^2e^{-i2Ky}\right\}dy+\frac{i}{2K}\sigma_3^2e^{-i2Ky_0(x)}\right]. \tag{A19}$$

Because this is the result after transformation of equation (A3), we can obtain from equations (A1) and (A2) the expression for an additional contribution to the added mass and damping coefficients for the case of $(j,k)=(3,5)$ and $(j,k)=(5,3)$ in the form given as follows:

$$A_{jk}+\frac{1}{i\omega}B_{jk}=-\rho i\omega U\int_L I_{jk}(x)dx=\mp\rho i2\frac{U\omega}{g}\int_L I(x)dx, \tag{A20}$$

where

$$I(x)\equiv\int_{y_0(x)}^{\infty}\left\{\varphi_3^2(y,0)+\sigma_3^2e^{-i2Ky}\right\}dy+\frac{i}{2K}\sigma_3^2e^{-i2Ky_0(x)}. \tag{A21}$$

This result is the expression given as equation (34) in the present article.